Relationships Between Aerosols and Precipitation in the Southern Appalachian Mountains

By: **P. T. Soule**, G. M. Kelly, B. F. Taubman, L. B. Perry, J. P. Sherman, and P. J. Sheridan

Abstract

There are many uncertainties associated with aerosol-precipitation interactions, particularly in mountain regions where a variety of processes at different spatial scales influence precipitation patterns. Statistical relationships between aerosols and precipitation were examined in the southern Appalachian Mountains to determine the seasonal and synoptic influences on these relationships, as well as the influence of air mass source region. Precipitation events were identified based on regional precipitation data and classified using a synoptic classification scheme developed for this study and published in a separate manuscript (Kelly et al. 2012). Hourly aerosol data were collected at the Appalachian Atmospheric Interdisciplinary Research (AppalAIR) facility at Appalachian State University in Boone, NC (1110 m asl, 36.215 ◦ , –81.680 ◦). Backward air trajectories provided information on upstream atmospheric characteristics and source regions. During the warm season (June–September), greater aerosol loading dominated by larger particles was observed, whereas cool season (November–April) precipitation events exhibited overall lower aerosol loading with an apparent influence from biomass burning particles. A significant relationship between aerosol optical properties and precipitation intensity was observed, which may be indicative of aerosol-induced precipitation enhancement in each season, particularly during warm season non-frontal precipitation.

P. T. Soule, G. M. Kelly, B. F. Taubman, L. B. Perry, J. P. Sherman, and P. J. Sheridan (2013) "Relationships Between Aerosols and Precipitation in the Southern Appalachian Mountains" *International Journal of Climatology* Volume. 33 pp. 3016-3028 Version of Record Available From (www.onlinelibrary.wiley.com)

1. Introduction

The interactions of aerosols, clouds, and precipitation are of particular concern in the southeastern United States (SEUS), where there is a high concentration of atmospheric aerosols of both natural and anthropogenic origin (Weber *et al.*, 2007). In the southern Appalachian Mountains (SAM), weather patterns are strongly influenced by topography and frontal activity associated with extra-tropical cyclones. While the major focus of this study is to investigate the association of aerosol properties with precipitation formation in the SAM, it is important to acknowledge there is a reciprocal relationship between aerosols and climate that remains poorly understood (Power *et al.*, 2006). Atmospheric aerosols influence weather and climate patterns by altering Earth's surface energy balance and impacting the microphysical processes of cloud formation and precipitation development. However, weather and climate patterns influence aerosol loading and ultimately the chemical, optical, and microphysical properties of aerosols on a variety of scales. This study examines the synoptic controls of precipitation patterns and aerosols in the SAM based on a synoptic classification scheme described by Kelly *et al.* (2012, accepted for publication in *Climate Research*).

Aerosol climatologies have been constructed based on the optical properties of aerosols produced by various sources, including biomass burning, desert dust, biogenic emissions, and anthropogenic sources (Holben *et al.*, 2001; Bollasina *et al.*, 2007). The transport of atmospheric particles from source regions to remote areas is an important component of global climate change research and incorporates processes of aerosol loading and synoptic climatology. Aerosol behaviours are affected by meteorological factors on a variety of scales: microscale climatic factors, such as insolation and humidity, can enhance conversion of gases into particles as well as the particle growth; atmospheric stability and convection at the mesoscale can often determine the concentration of aerosols in the atmosphere; and at the synoptic scale, source region and variable flow patterns dictate the presence and concentration of atmospheric aerosols (Power *et al.*, 2006). A variety of methodologies have been used in evaluating the synoptic controls of atmospheric aerosols, including ground-based sampling schemes (Power *et al.*, 2006) as well as backward air trajectory analyses (Dorling *et al.*, 1992; Swap *et al.*, 1992; Prados *et al.*, 1999; Brankov *et al.*, 1998; Taubman *et al.*, 2006).

Numerous studies have addressed aerosol-induced precipitation enhancement (Rosenfeld *et al.*, 2002; Rudich and Khersonsky, 2002; Givati and Rosenfeld, 2004; Khain *et al.*, 2004; Bell *et al.*, 2008; Lohmann and Hoose, 2009) and precipitation suppression (Rosenfeld, 2000; Borys *et al.*, 2003; Andreae *et al.*, 2004; Rosenfeld and Givati, 2006). Aerosols strongly impact the precipitation potential of shallow stratiform clouds that occur below (i.e. under) the -10°C isotherm (Rosenfeld, 1999, 2000). The precipitation potential of warmer clouds has been shown to decrease with an increased number of aerosols; however, cloud glaciation processes in mixed-phase clouds may compensate for this effect in mountainous regions (Zubler *et al.*, 2011). It has been observed that orographic clouds are particularly sensitive to the indirect effects of anthropogenic aerosols due to their shallow vertical structure and downwind termination (Borys *et al.*, 2003; Givati and Rosenfeld, 2004, 2005; Jirak and Cotton, 2005; Rosenfeld and Givati, 2006; Rosenfeld *et al.*, 2007).

This study provides results from 16 months of continuous surface-based aerosol measurements at a high elevation site just below the typical cloud base height in the SEUS and constitutes the first attempt to identify statistical relationships between aerosols and precipitation in the SAM, information that may enhance weather forecasts and modelled future climate scenarios. There is a reciprocal relationship between aerosols and climate wherein changes in climate affect aerosol properties, while changes in aerosol properties affect climate patterns (Power *et al.*, 2006). It is yet to be fully understood how changes in aerosol properties affecting the SAM may influence atmospheric processes across the region and impact weather and climate patterns as a result.

Currently, global climate models (GCMs) are not equipped to sufficiently parameterize aerosols in order to account for their direct and indirect effects on weather and climate patterns (Power *et al.*, 2006). Current circulation models project increased variability in precipitation patterns in the SEUS, indicating more intense periods of deluge and drought, as a result of anthropogenic-induced warming (Lynn *et al.*, 2007; Karl *et al.*, 2009; Li *et al.*, 2010). However, the physical processes of aerosol-precipitation interactions and the topographic influences on precipitation are not well understood and are difficult to represent in GCMs (Power *et al.*, 2006). Changes in atmospheric circulation patterns may lead to synoptic-scale conditions that enhance aerosol loading in the SAM. The climatological summer (JJA: June–July–August) of 2010 was one of the hottest periods on record for many regions in the SEUS, and it is projected that the region may become drier and warmer in the coming decades (Karl *et al.*, 2009; Li *et al.*, 2010).

The primary goals of this study are to investigate the statistical relationships between aerosols and precipitation in the SAM by addressing the following research questions: (1) How do aerosol properties observed during precipitation events vary by season (e.g. summer *vs* winter) and synoptic event type (e.g. frontal *vs* non-frontal) and (2) What influence does air mass source region have on aerosol properties? A synoptic classification scheme (Kelly *et al.*, 2012) was created to classify precipitation events during 2009–2010 in the SAM and summarize them by their synoptic influences. Precipitation events were summarized by seasonal and synoptic variations in aerosol properties. This study adds to current scientific knowledge by presenting statistical relationships between aerosols and precipitation in an area that experiences the orographic enhancement of precipitation. The methods and results of this study may be applicable in aerosol-precipitation studies in other mountainous regions of the world.

2. Data and methods

2.1. Precipitation data and event identification

The study area was centred on the Appalachian Atmospheric Interdisciplinary Research (AppalAIR) facility (36.213°, -81.691°; 1110 m) on the campus of Appalachian State University (ASU) in Boone, NC (Figure 1). Daily precipitation totals at monitoring stations within the study area were analyzed during the period 01 June–30 September in 2009 and 2010 (i.e. warm seasons) and 01 November 2009–30 April 2010 (i.e. cool season). Warm season and cool season events were separated due to the spatial and temporal variability in the stability, synoptic patterns associated with precipitation development, and aerosol loading and type characteristic of each season (Konrad, 1997). The shoulder months of May and October were omitted from this study.

Periods of precipitation were identified from the Boone Automated Weather Observing System (AWOS) hourly weather-type data and corroborated with hourly precipitation data from the Boone Environmental and Climate Observing Network (ECONet) station and daily precipitation totals from the Boone cooperative observer (COOP) station and the Community Collaborative Rain, Hail, and Snow (CoCoRaHS) network stations (Cifelli *et al.*, 2005) in the town of Boone. Precipitation data were obtained and compiled for analysis from 59 monitoring stations in the CoCoRaHS network and from 16 monitoring stations in the COOP network located above 305 m elevation (Figure 1). Events that qualified for this study produced measurable precipitation ($\geq$0.25 mm) at one or more of the aforementioned monitoring stations. Events were distinguished from one another by a 6-h time period of no precipitation, and the timing of each event was characterized in terms of beginning, maturation, and ending times based on Boone AWOS hourly weather-type data and consistent with the approach used by Perry *et al.* (2007, 2010) in their investigations of snowfall in the SAM. The beginning of an event was defined as the hour corresponding with the first report of precipitation of any kind, with a minimum of 6 h of no precipitation beforehand; the maturation of an event was defined as the hour corresponding with the heaviest precipitation reports; and the

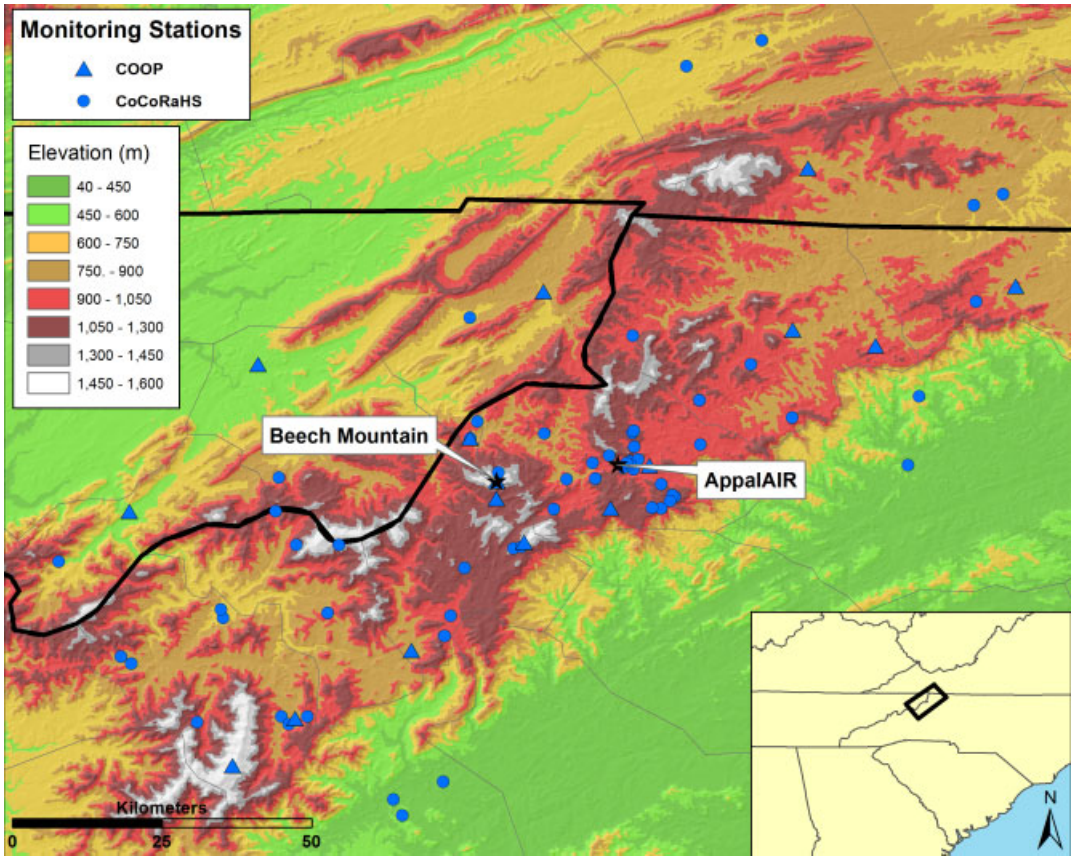

Figure 1. Topography of study area, including locations of AppalAIR, Beech Mountain, and COOP and CoCoRaHS stations.

ending of an event was defined as the hour corresponding with the last report of precipitation of any kind.

2.2. Synoptic classification

Events were classified using a synoptic classification scheme developed for this study (Kelly *et al.*, 2012) and adapted from Keim (1996). Events took place between 01 June and 30 September were defined as warm season events and those between 01 November and 30 April were defined as cool season events. Events were further classified as frontal or non-frontal events based on archived three-hourly National Centers for Environmental Prediction (NCEP) Service Records Retention System (SRRS) Analysis and Forecast Charts (National Climatic Data Center Service Records Retention System Analysis and Forecast Charts, 2010) and NCEP daily weather maps (National Centers for Environmental Prediction Daily Weather Maps, 2012). Frontal and non-frontal precipitation events were differentiated due to the synoptic influences on moisture and aerosols. Frontal events were identified by the presence of a frontal boundary within 300 km of the study area, and were identified as cold, warm, stationary, or occluded, based on SRRS and NCEP weather charts. In the absence of a clear frontal boundary within 300 km of the study area, events were identified as Gulf Lows when precipitation was associated with a low pressure centre in the Gulf of Mexico and as Nor'easters if precipitation was associated with a surface cyclone tracking to the northeast. Nor'easters were sometimes associated with a 500 hPa low pressure centre passing nearby the study area. Non-frontal events were defined as precipitation occurring in the absence of frontal activity within 300 km from the study area, and these events included convective and orographic processes of precipitation development.

Events were further classified based on spatial coverage. If $<75\%$ of active stations reported measurable precipitation, the events were classified as scattered, whereas if $\geq 75\%$ of active stations reported measurable precipitation, the events were classified as widespread. Additionally, events were analyzed according to upper and lower quartile precipitation values, creating subcategories of events representing heavy and light precipitation, respectively.

2.3. Meteorological data

Meteorological data were collected from the Beech Mountain monitoring station (36.185°, −81.881°; 1678 m), located approximately 17.4 km west of AppalAIR (Figure 1). Average temperature, relative humidity, wind speed, and wind direction values were collected from the State Climate Office of North Carolina Climate Retrieval and Observations Network of the Southeast (CRONOS) and were compiled for beginning and maturation hour of

each event and summarized by event type. Average wind direction values were calculated as unit-vector averages, and most frequent wind directions were determined by analysis of a histogram of observed wind directions during each event. In contrast to Boone and other valley or ridge-top locations, wind direction at Beech Mountain is not considerably controlled by local topography, and data from this location are therefore broadly representative of lower tropospheric (~825 hPa) meteorological conditions. Meteorological data from the Beech Mountain meteorological station (BEECHTOP) were not available from 26 December 2009 through 10 January 2010 due to severe ice and wind causing catastrophic tower collapse.

2.4. Aerosol data

The AppalAIR site has been a NOAA/Earth System Research Laboratory (NOAA/ESRL) Global Monitoring Division (GMD) Collaborative Surface Aerosol Monitoring Network site since 01 June 2009. Because of the height of the tree canopy at the site, aerosol samples are collected from the top of a 34 m above ground level (agl) sample inlet (~20 cm internal diameter). As a result, the AppalAIR site is typically only 300–500 m below the cloud base and measurements are believed to be representative of the bottom of the moist layer, which is significant in sampling feeder clouds related to orographic precipitation processes. The aerosol sampling protocol used is the same one employed at all NOAA-ESRL collaborative aerosol monitoring sites (Sheridan *et al.*, 2001). The inlet is outfitted with a stainless rain cap and mesh screen to keep birds and insects out. Total flow through the stack is ~1 $m^3\,min^{-1}$. Roughly 150 $L\,min^{-1}$ is taken from the centre of the main stack and directed through a stainless tube (~5 cm internal diameter) to supply the instruments in the facility. This inlet is heated to maintain a RH of ≤50% prior to entering the facility. Once inside the facility, the inlet is heated second time to decrease the RH to ≤40% and divided into five individual sampling lines at 30 $L\,min^{-1}$. The remaining flow is either directed to additional instrumentation that will not be discussed in this paper or is exhausted through a blower and filter outside the facility.

Size-segregated aerosol light scattering and absorption is measured with a switched impactor system. A solenoid valve is used to switch the flow every 10 min between 1-μm aerodynamic diameter cutpoint and 10-μm aerodynamic diameter cutpoint multiple orifice impactors to achieve 1- ($D_p < 1$ μm) and 10-μm ($D_p < 10$ μm) size cuts. Size-segregated aerosol scattering and absorption coefficients (for particles with aerodynamic diameters <10 and <1 μm) were measured using a three-wavelength (450, 550, and 700 nm) integrating nephelometer (TSI Model 3563) and a three-wavelength (467, 530, and 660 nm) Particle Soot Absorption Photometer (PSAP, Radiance Research, Inc.), respectively. Absorption values were corrected for instrument-specific differences in flow rate, spot size, and also for aerosol scattering and filter matrix influences (Bond *et al.*, 1999). The nephelometer was calibrated with CO_2 and particle-free air and corrections were made to account for angular non-idealities within the nephelometer (Anderson and Ogren, 1998).

All aerosol properties used in this study (Table 1) were for the sub-10 μm particles, as this size limit accounted for the optical properties of virtually all aerosols measured at AppalAIR. Average aerosol properties during the 6 h prior to event beginning were analyzed in order to

Table 1. Instruments and aerosol measurements made at AppalAIR. Absorption Ångström exponent value calculated using based on Delene and Ogren (2002).

Instrument	Primary measurement	Derived measurements	Description of intensive property
TSI Model 3563 three-wavelength (450, 550, and 700 nm) integrating nephelometer	Total scattering and hemispheric backscattering coefficients (σ_{sp} and σ_{bsp}) at 450, 550, 700 nm, for particles with aerodynamic diameters <10 and <1 μm	Hemispheric backscatter fraction, $b = \sigma_{bsp}/\sigma_{sp}$	b provides a qualitative indicator of particle size, with higher (lower) values corresponding to smaller (larger) particles
		Single scattering albedo at 550 nm, $\omega_o = \sigma_{sp}/(\sigma_{sp} + \sigma_{ap})$	ω_o provides an indicator of the relative contributions of absorption and scattering to total light extinction
		Scattering Ångström exponent, $\alpha_{scat} = -\log[\sigma_{sp}(450)/\sigma_{sp}(700)]/\log[450/700]$	α_{scat} is a measure of the spectral dependence of aerosol light scattering, providing a means for broadly classifying aerosol size
Radiance Research three-wavelength (467, 530, 660 nm) Particle Soot Absorption Photometer (PSAP)	Light absorption coefficient (σ_{abs}) at 467, 530, and 660 nm, for particles with aerodynamic diameters <10 and <1 μm	Absorption Ångström exponent, $\alpha_{abs} = -\log[\sigma_{abs}(467)/\sigma_{abs}(660)]/\log[467/660]$ (Delene and Ogren, 2002)	α_{abs} is a measure of the spectral dependence of aerosol light absorption, providing a means for broadly classifying aerosol types

determine patterns in these values leading up to the onset of precipitation. Aerosol properties were also analyzed during the beginning and maturation times of each event.

2.5. Trajectory analysis

The NOAA Air Resources Laboratory (ARL) HYbrid Single-Particle Lagrangian Integrated Trajectory (HYSPLIT) model (version 4) (Draxler and Rolph, 2011) and 40 km Eta Data Assimilation System (EDAS) three-hourly archive data were used to create 72-h, three-dimensional kinematic backward air trajectories ending at maturation time of each event at the coordinate location of AppalAIR (36.213°, −81.691°). To account for seasonal surface-atmosphere interactions in the lower troposphere at ∼800 hPa, warm season trajectories were run with an ending height at 2000 m above sea level (asl), and cool season trajectories were run at 1500 m asl.

For each synoptic class, a cluster analysis was performed on the backward air trajectories associated with the maturation hour of each precipitation event, an approach based on the clustering methodology used by Taubman *et al.* (2006). HYSPLIT uses multiple iterations to create clusters of trajectories by calculating the total spatial variance (TSV) among trajectories. In the first iteration, TSV is zero and each trajectory is considered a stand-alone cluster at this stage (i.e. N trajectories = N clusters) (Draxler, 1999). Two trajectories are paired and the cluster spatial variance (SPVAR) is calculated, which is the sum of the squared distances between the endpoints of the paired clusters. TSV is then calculated, which is the sum of all cluster spatial variances, and pairs of clusters that are combined are those with the lowest increase in TSV. For the second iteration, the number of clusters is N – 1 since two trajectories were clustered together in the first iteration, resulting in one less stand-alone cluster. The same calculations and comparisons were performed, resulting in the combination of the two clusters with the lowest increase in TSV. Iterations continue until the very last two clusters are combined. After several iterations during the cluster analysis, TSV increases rapidly, indicating that trajectories being combined within the same cluster are not very similar. At this stage, clustering should stop. In a plot of TSV *versus* number of clusters, the step just before the large increase in TSV indicates the final number of clusters. While some subjectivity was involved in the choice of final number of clusters, a large change in TSV was required and the choice was not arbitrary.

2.6. Statistical tests

All datasets were tested for normality ($\alpha = 0.05$) using the Kolmogorov–Smirnov test. For data that were not normally distributed, differences of means were tested ($\alpha = 0.05$) using the Mann–Whitney U two-sample rank sums test (non-parametric). When normally distributed, an independent sample t-test (parametric) was used. Differences of means of meteorological and aerosol values were tested for each event type, and comparisons were made between seasons, and also among different event types within the same season. Precipitation events were also analyzed in terms of upper and lower quartile precipitation values (i.e. heavy and light precipitation events) and the corresponding aerosol values in order to assess the pattern of aerosols associated with light precipitation *versus* heavy precipitation. Aerosol values at the beginning-6 h and maturation hour of each event were analyzed separately. Aerosol values at the beginning-6 h of each event indicated the properties of aerosols before heavy precipitation set in, giving information about aerosol loading and the potential for impacting precipitation. Values at maturation indicated the interaction of aerosols with precipitation in terms of a possible raining out effect. As a result, the differences in values from beginning-6 h to maturation were analyzed.

3. Results and discussion

3.1. Synoptic classification

The synoptic classification scheme resulted in 183 precipitation events during the study period (Figure 2) (Kelly *et al.*, 2012). There were 123 events during the two warm seasons in the study period, which included precipitation associated with cold, warm, and stationary fronts, as well as non-frontal mechanisms involving shallow upslope flow and terrain-induced convection. Warm season precipitation events lasted an average of 5 h, ranging in duration from 1 to 29 h, and producing an average of 8.9 mm of precipitation. Overall, these precipitation events were characterized by the presence of the North American Subtropical High (NASH) to the east (e.g., Li *et al.*, 2010), which favoured precipitation in the SEUS by the advection of moisture from the Atlantic Ocean and the Gulf of Mexico and resulted in dominant wind directions from the south and northwest (Table 2). During the warm season, the majority of air masses had a Gulf or Atlantic Ocean coastal connection and therefore higher moisture flux (Figure 2).

There were 60 cool season precipitation events, which included frontal precipitation associated with cold, warm, and occluded fronts, as well as Gulf Lows and Nor'easters (Kelly *et al.*, 2012). Non-frontal mechanisms, such as northwest upslope flow (e.g., Keighton *et al.*, 2009; Perry *et al.*, 2007) were also responsible for some events. Cool season precipitation events exhibited an overall longer duration than warm season events, lasting an average of 16 h and ranging in duration from 1 to 66 h, and producing an average of 13.4 mm of precipitation. Cool season precipitation events were associated with lower pressures over the study area and to the northeast, with higher pressures to the west, suggesting the advection of air from inland areas and much less moisture originating in the Gulf of Mexico or the Atlantic Ocean. Most air masses associated with cool season precipitation events originated west of the study area (Figure 2), with dominant wind directions from the northwest and south-southeast (Table 2).

Figure 2. HYSPLIT cluster analysis of backward air trajectories representing maturation hour of each precipitation event during warm season (top) and cool season (bottom). Coloured lines represent the mean trajectory of each cluster. Clusters are numbered and values in parentheses represent the percentage of backward air trajectories included in each cluster. Trajectories terminating before 72 h, likely as a result of missing meteorological data, were not included in the clustering.

3.2. Aerosol classification

3.2.1. Seasonal variation

Meteorological variables and aerosol properties at beginning and maturation associated with each cluster reveal distinct differences in source region influences during warm season and cool season precipitation events. Scattering values were much higher during warm season precipitation events (Table 3), consistent with the overall regional increase in secondary organic aerosols during this season (Goldstein *et al.*, 2009). Cool season events were characterized by higher b, α_{scat}, and α_{abs} (Table 1) values, consistent with the presence of locally emitted biomass burning particles (Bergstrom *et al.*, 2002) from wood-burning stoves, which serve as the primary heating source for 6.2% of occupied housing units in Watauga County (U.S. Census Bureau, 2010) (Table 3).

Synoptic influences and increased scattering and absorption coefficients during warm season precipitation events resulted in significant differences in aerosol values between warm season and cool season precipitation (Table 3). Higher scattering values are driven by secondary organic aerosols during the warm season (Barr *et al.*, 2003), and the presence of overall larger

Table 2. Seasonal summaries of precipitation events. Average total precipitation values from COOP and CoCoRaHS stations in study area. Average temperature, relative humidity, wind speed, and wind direction are from the BEECHTOP meteorological station.

Season	n	Average spatial coverage (%)	Avg. total precip. (mm)	Temperature (°C)	Relative humidity (%)	Wind speed (m/s)	Wind direction (°)	Most frequent wind direction(s) (°)
Warm	123	80	8.9	15.8	95.6	3.4	244 (SW)	S, NW
Cool	60	69	13.4	−1.6	98.0	5.0	172 (S)	SSE, NW

Table 3. Differences in mean meteorological and aerosol values at beginning-6 h and maturation for all warm season events *versus* all cool season precipitation events, plus difference in values from beginning-6 h to maturation.

	All warm $n = 123$	All cool n = 60	Abs. diff.	p-value
Avg. precip. (mm)	8.9	13.6	4.7	0.945

	Beginning-6 h				Maturation				Diff. from beg.-6-mat.	
	All warm	All cool	Abs diff	p-value	All warm	All cool	Abs diff	p-value	All warm	All cool
Meteorological values									*p-value*	*p-value*
Beech T (°C)	16.3	−1.1	17.4	***0.000****	15.3	−2.2	17.5	***0.000****	***−0.006****	−0.416*
Beech RH (%)	92.4	90.2	2.2	0.721	96.2	98.8	2.6	0.205	***+0.000***	***+0.000***
Beech WS (m/s)	7.5	10.7	3.2	***0.001***	3.7	5.7	2.1	***0.004***	+0.107	+0.487
Beech WD (°)	232 (SW)	195 (SSW)	37	NA	244 (WSW)	176 (S)	68	NA	NA	NA
Aerosol values										
Scattering	57.43	28.24	29.19	***0.000***	45.08	16.58	28.50	***0.000***	***−0.002***	***−0.001***
Absorption	3.49	3.71	0.22	0.566	3.20	2.40	0.80	***0.002***	***−0.003***	***−0.001***
b	0.12	0.15	0.03	***0.000***	0.13	0.16	0.04	***0.000***	+0.237	+0.101
ω_o	0.93	0.87	0.06	***0.000***	0.92	0.84	0.07	***0.000***	−0.329	−0.222
α_{scat}	1.97	2.07	0.10	***0.003***	1.95	2.16	0.21	***0.000***	−0.565	***+0.003***
α_{abs}	0.42	0.95	0.53	***0.000****	0.58	1.20	0.62	***0.000****	***+0.000****	***+0.000****

p-values (two-tailed) italicized in bold indicate significance at the 95% confidence interval or greater.
An asterisk (*) indicates values obtained using a parametric test.

particles during this time of year at event beginning and maturation is evidenced by significantly smaller b and α_{scat} values. The larger warm season ω_o (Table 1) values indicated the presence of relatively greater scattering, likely the result of increased biogenic emissions in the SEUS (Goldstein *et al.*, 2009). Smaller warm season α_{abs} values suggest the presence of relatively more soot-like carbonaceous particles during this time of year and less biomass burning particles, whereas larger α_{abs} values during the cool season were consistent with the presence of biomass burning aerosols (Bergstrom *et al.*, 2002) possibly emitted locally as a result of winter wood burning in the SAM.

There was a significant decrease in both scattering and absorption coefficients from 6 h prior to the beginning of the event (beginning-6 h) to maturation during warm and cool season precipitation events, which was consistent with a raining out effect that removed particles from the air during precipitation (Table 3). A significant increase in α_{abs} from beginning to maturation was displayed in both seasons, possibly the result of low vapour pressure water soluble organic carbon coalescing with the existing particles as relative humidity increased. It is also possible that the increase in α_{abs} at maturation was a result of the atmospheric aging and mixing of black carbon particles, advected from some distance away, with locally emitted sulphate. This would cause black carbon particles to become coated in sulphate and subsequently more hygroscopic than freshly emitted organics and more effective at scattering light as a result of the collection of more scattering materials and a change in fractal shape.

Light warm season precipitation was associated with significantly cooler and windier conditions than heavy warm season precipitation (Table 4). Heavy warm season precipitation events displayed significantly lower α_{scat} and higher α_{abs} values (yet not a large difference) during maturation than light events, suggesting a greater presence of larger and more organic particles during periods of heaviest rainfall (Table 4). Heavy warm season precipitation also exhibited significantly higher α_{abs} values during maturation relative to beginning-6 h, indicating that a higher fraction of organic aerosols [effective cloud condensation nuclei (CCN)] relative to soot particles (ineffective CCN) may have enhanced the precipitation intensity in the SAM. That is, during the warm season when there was a relatively larger fraction of soot, differences in the amount of hygroscopic secondary organic aerosols serving as effective CCN may have intensified precipitation. The fact that optical properties suggested there was a greater fraction of biomass burning aerosols relative to soot during maturation of cool season precipitation (Table 5) likely decreased the importance of variability in these aerosols to precipitation intensity.

Table 4. Differences in mean meteorological and aerosol values at beginning-6 h and maturation between light *versus* heavy warm season precipitation events, plus difference in values from beginning-6 h to maturation.

	Light	Heavy	Abs. diff.	p-value
	$n = 31$	$n = 31$		
Avg. Precip. (mm)	2.1	20	17.9	***0.000****

	Beginning-6 h				Maturation				Diff. from beg.-6-mat.	
	Light	Heavy	Abs. diff.	p-value	Light	Heavy	Abs. diff.	p-value	Light	Heavy
Meteorological values									p-value	p-value
Beech T (°C)	14.4	15.4	1.0	***0.012****	14.4	15.4	1.0	0.187*	−0.423*	−0.084*
Beech RH (%)	96.0	95.7	0.3	0.224	96	95.7	0.3	0.844	***+0.012***	***+0.002***
Beech WS (m/s)	4.1	3.8	0.3	***0.007****	4.1	3.8	0.3	0.563*	+0.997*	+ 0.060
Beech WD (°)	232 (SW)	215 (SW)	17	NA	254 (WSW)	184 (S)	70	NA	NA	NA
Aerosol values										
Scattering	56.43	59.09	2.66	0.863	51.17	34.59	16.58	***0.012***	−0.483*	***−0.016***
Absorption	3.45	3.35	0.10	0.791*	3.51	2.83	0.68	0.149	+0.917*	***−0.035***
b	0.13	0.12	0.01	0.388*	0.13	0.13	0.00	0.835	−0.829	+0.200
ω_o	0.93	0.91	0.02	0.669	0.93	0.88	0.05	0.276	−0.676*	−0.437
α_{scat}	2.04	1.96	0.08	0.147*	2.05	1.92	0.13	***0.022****	+0.718	−0.341*
α_{abs}	0.40	0.41	0.01	0.917*	0.48	0.70	0.22	***0.016****	+0.265*	***+0.004****

p-values (two-tailed) italicized in bold indicate significance at the 95% confidence interval or greater.
An asterisk (*) indicates values obtained using a parametric test.

Table 5. Differences in mean meteorological and aerosol values at beginning-6 h and maturation between light *versus* heavy cool season precipitation events, plus difference in values from beginning-6 h to maturation.

	Light	Heavy	Abs. diff.	p-value
	$n = 15$	$n = 15$		
Avg. precip. (mm)	1.3	39.3		***0.000****

	Beginning-6 h				Maturation				Diff. from beg.-6-mat.	
	Light	Heavy	Abs. diff.	p-value	Light	Heavy	Abs. diff.	p-value	Light	Heavy
Meteorological values									p-value	p-value
Beech T (°C)	−4.5	3.1	7.6	***0.001***	−4.8	2.6	7.4	***0.001****	+0.974*	−0.802*
Beech RH (%)	96.9	80.5	16.4	***0.002***	99.1	99.9	0.88	0.062	+0.325	***+0.000***
Beech WS (m/s)	3.5	7.2	3.7	***0.004***	3.4	9.5	6.1	***0.001****	−0.612	+0.177*
Beech WD (°)	286 (W)	163 (SSE)	123	NA	256 (WSW)	142 (SE)	114	NA	NA	NA
Aerosol values										
Scattering	16.09	42.42	26.33	***0.058***	14.28	15.95	1.67	0.835	−0.724	***+0.000***
Absorption	1.82	5.90	4.08	***0.000****	2.75	2.36	0.39	0.297	+0.983	***+0.000***
b	0.15	0.14	0.01	0.193*	0.17	0.16	0.01	0.531	+0.576	+0.099*
ω_o	0.87	0.86	0.01	***0.021***	0.82	0.83	0.01	0.531	−0.950	***−0.008***
α_{scat}	2.08	1.98	0.10	0.121*	2.19	1.97	0.22	0.192*	+0.215*	−0.959*
α_{abs}	0.91	0.99	0.08	0.132*	1.24	1.28	0.04	0.669*	***+0.000****	***+0.001****

p-values (two-tailed) italicized in bold indicate significance at the 95% confidence interval or greater.
An asterisk (*) indicates values obtained using a parametric test.

3.2.2. *Synoptic variation*

While influenced by very different air mass source regions during the time period of this study (Figure 3), analysis revealed no significant differences in the meteorological characteristics or aerosol values associated with warm season frontal and non-frontal precipitation events. There was, however, a significant increase in α_{abs} values from beginning-6 h to maturation during precipitation associated with each synoptic type during the warm season, which was consistently seen throughout this study (Table 6). During warm season frontal precipitation, scattering decreased significantly from beginning-6 h to maturation, evidence of particles being rained out. However, during warm season non-frontal precipitation, absorption decreased significantly from beginning-6 h to maturation (Table 6).

There were no significant differences in precipitation between lower and upper quartile aerosol values during warm season frontal precipitation events (Table 7). This may be a result of a 'snowplow' effect, in which the leading edge of a frontal boundary accumulates aerosols while approaching the SAM, leading to similar aerosol loading during both light and heavy frontal precipitation events in the warm season. Precipitation totals associated with upper and lower quartile aerosol values did exhibit significant differences during warm season non-frontal precipitation events (Table 7). During maturation, warm

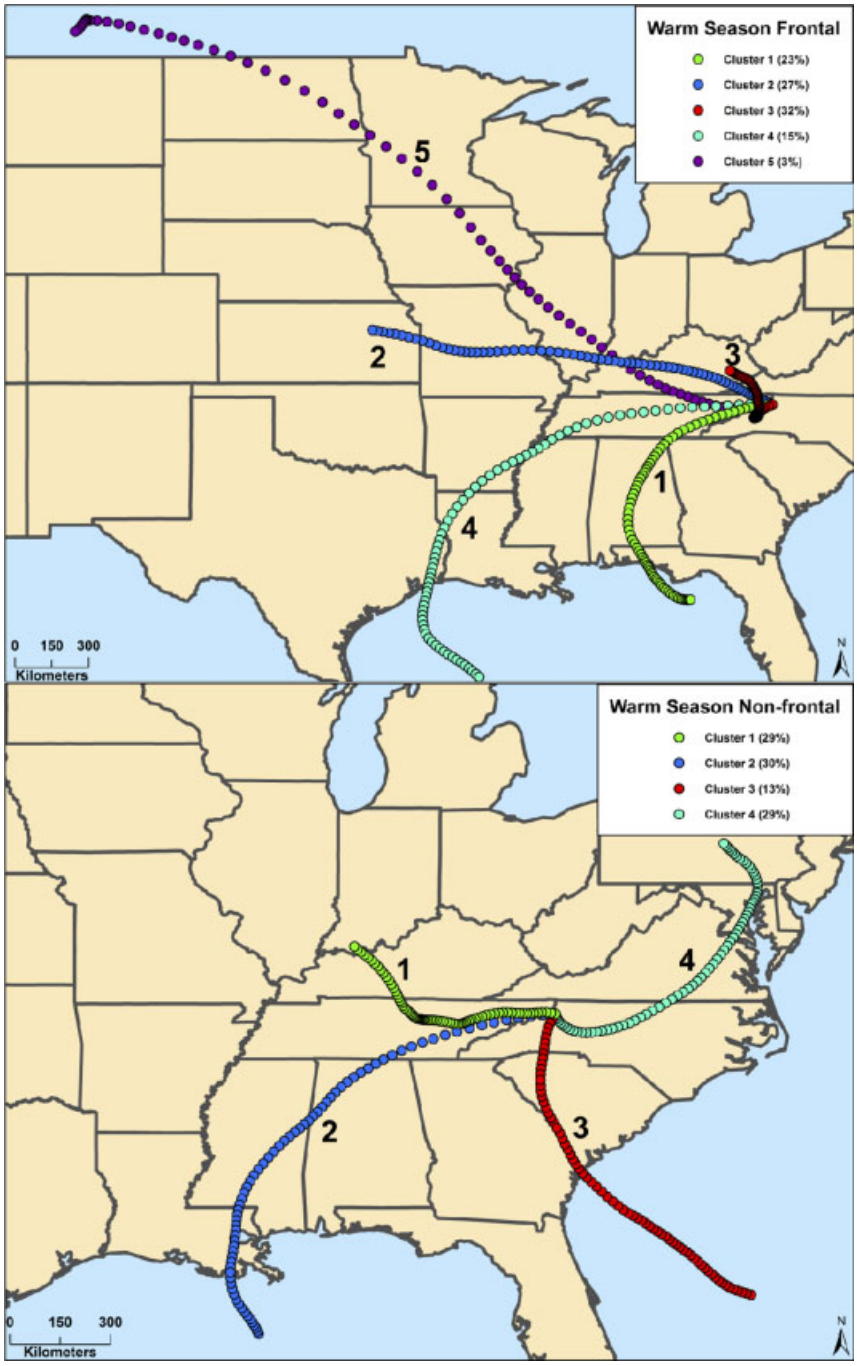

Figure 3. HYSPLIT cluster analysis of backward air trajectories representing maturation hour of warm season frontal (top) and non-frontal (bottom) precipitation events. Coloured lines represent the mean trajectory of each cluster. Clusters are numbered and values in parentheses represent the percentage of backward air trajectories included in each cluster.

season non-frontal precipitation events exhibited significantly higher precipitation totals associated with higher scattering and α_{abs} values and lower α_{scat} (Figure 4). Aerosol properties at AppalAIR are monitored at an elevation that is very close to the cloud base. Thus, the presence of secondary organic aerosols is recorded, and these aerosols can serve as effective CCN in the SEUS during the warm season (Goldstein *et al.*, 2009).

Analysis of light and heavy warm season non-frontal precipitation revealed significantly lower α_{scat} values during heavy events at beginning-6 h. (Table 8), possibly suggesting the presence of larger organic particles serving as effective CCN during heavy precipitation *versus* light precipitation. There was no significant change in b at maturation between light and heavy warm season non-frontal precipitation, indicating a questionable difference in particle size between these event types; however, scattering and α_{scat} values were significantly lower during heavy events, accompanied by higher α_{abs} values, all of which may indicate the presence of hygroscopic organic

Table 6. Differences in mean meteorological and aerosol values at beginning-6 h and maturation between warm season frontal and non-frontal precipitation events, plus difference in values from beginning-6 h to maturation.

	Warm frontal	Warm non-frontal	Abs. diff.	p-value
	$n = 60$	$n = 63$		
Avg. precip. (mm)	10.2	7.6	2.6	0.231

	Beginning-6 h				Maturation				Diff. from beg.-6-mat.	
	Warm frontal	Warm non-frontal	Abs. diff.	p-value	Warm frontal	Warm non-frontal	Abs. diff.	p-value	Warm frontal	Warm non-frontal
Meteorological values									p-value	p-value
Beech T (°C)	16.1	16.4	0.3	0.575*	14.9	15.7	0.8	0.110*	***−0.013****	−0.139*
Beech RH (%)	93.3	91.6	1.7	0.312	97.6	94.9	2.7	0.071	***+0.000***	***+0.000***
Beech WS (m/s)	7.8	7.3	0.5	0.445	3.8	3.5	0.4	0.256*	−0.177	−0.336
Beech WD (°)	248 (WSW)	213 (SSW)	35	NA	271 (W)	207 (SSW)	64	NA	NA	NA
Aerosol values										
Scattering	53.38	61.23	7.85	0.137	39.40	50.11	10.71	0.072	***−0.012***	−0.066*
Absorption	3.20	3.75	0.55	0.094	3.20	3.19	0.01	0.255	+0.050	***−0.017***
b	0.12	0.12	0.00	0.065	0.13	0.12	0.01	0.165	+0.582	+0.293
ω_o	0.93	0.93	0.00	0.945	0.92	0.92	0.00	0.352	−0.224	−0.897
α_{scat}	1.99	1.95	0.04	0.285	1.97	1.92	0.05	0.284*	−0.771	−0.513*
α_{abs}	0.44	0.41	0.03	0.610*	0.60	0.57	0.04	0.563*	***+0.010****	***+0.006****

p-values (two-tailed) italicized in bold indicate significance at the 95% confidence interval or greater.
An asterisk (*) indicates values obtained using a parametric test.

Table 7. Mean precipitation (mm) values associated with lower and upper quartile aerosol values during warm season frontal and non-frontal precipitation events.

	Beginning-6 h				Maturation			
Aerosol values	Lower ($n = 15$) Precip.	Upper ($n = 15$) Precip.	Abs. diff.	p-value	Lower ($n = 15$) Precip.	Upper ($n = 15$) Precip.	Abs. diff.	p-value
Frontal precipitation events								
Scattering	10.0	12.0	2.0	0.777	7.6	13.0	5.4	0.232
Absorption	11.6	6.6	5	0.394	8.3	11.8	3.5	0.801
b	6.9	10.2	3.3	0.192	10.6	9.2	1.4	0.783
ω_o	9.1	10.3	1.2	0.301	9.0	11.8	2.8	0.804
α_{scat}	5.1	9.8	4.7	0.077	9.3	10.1	0.8	0.646
α_{abs}	8.3	8.2	0.1	0.957	10.5	10.5	0.0	0.762
Non-frontal precipitation events								
Scattering	6.5	7.3	0.8	0.678	1.2	5.5	4.3	***0.017***
Absorption	8.8	7.6	1.2	0.527	8.2	5.2	3.0	0.224
b	14.9	17.0	2.1	0.533*	6.2	7.7	1.5	0.838
ω_o	7.5	4.6	2.9	0.060	1	5.8	4.8	0.160
α_{scat}	7.5	4.6	2.9	0.136*	8.7	3.7	5.0	***0.001***
α_{abs}	6.5	9.9	3.4	0.073	6.1	12.6	6.5	***0.010***

aerosols acting as effective CCN during increased warm season non-frontal precipitation (Table 8).

4. Summary

Relationships between aerosols and precipitation in the SAM were analyzed by identifying precipitation events based on regional precipitation data and classified using a synoptic classification scheme developed for this study. Hourly aerosol data were analyzed for each precipitation event to determine seasonal synoptic differences in aerosol optical properties during precipitation events, and backward air trajectory analysis revealed moisture and aerosol source region information.

Average precipitation per event during the warm season was lower than during the cool season. Warm season precipitation events exhibited a wide range of air mass source regions, with a large portion of the low-level moisture associated with warm season precipitation originating in coastal areas. Warm season precipitation events were associated with larger and more scattering aerosols, which in turn are related to phenological and meteorological cycles. Aerosol optical properties consistent with the presence of hygroscopic secondary organic aerosols acting as effective CCN were associated with warm season precipitation events, particularly during non-frontal mechanisms, which may be indicative of aerosol-induced precipitation enhancement. Analyses of the relationship

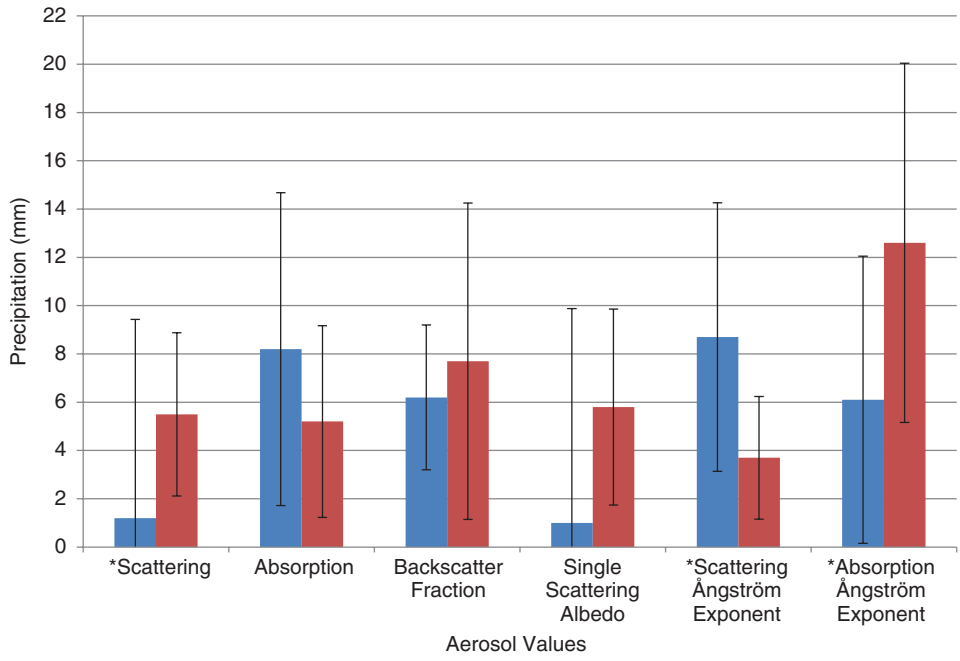

Figure 4. Precipitation values (with standard deviation bars) associated with lower (light gray) and upper (dark gray) quartile aerosol values observed during warm Season non-frontal precipitation events. Asterisk (*) indicates a difference in precipitation significant at the 95% confidence interval or greater.

Table 8. Differences in mean meteorological and aerosol values at beginning-6 h and maturation between light and heavy warm season non-frontal precipitation events, plus difference in values from beginning-6 h to maturation.

	Warm non-frontal light	Warm non-frontal heavy	Abs. diff.	p-value
	$n = 16$	$n = 16$		
Avg. precip. (mm)	2.1	16.4	14.3	***0.000***

	Beginning-6 h				Maturation				Diff. from beg.-6-mat.	
	Warm non-frontal light	Warm non-frontal heavy	Abs. diff.	p-value	Warm non-frontal light	Warm non-frontal heavy	Abs. diff.	p-value	Warm non-frontal light	Warm non-frontal heavy
Meteorological values									p-value	p-value
Beech T (°C)	15.6	16.1	0.5	0.617*	15.4	15.3	0.1	0.921*	0.972*	−0.612*
Beech RH (%)	91.8	94.0	2.2	0.817	93.1	96.9	3.8	0.601	−0.982	0.153
Beech WS (m/s)	3.8	3.4	0.4	0.228	3.7	4.1	0.4	0.499*	+0.945*	+0.551*
Beech WD (°)	184 (S)	195 (SSW)	11	NA	182 (S)	170 (S)	12	NA	NA	NA
Aerosol values										
Scattering	65.77	54.42	11.35	0.373*	58.67	30.43	28.24	***0.006****	−0.970	−0.199*
Absorption	3.93	3.56	0.37	0.309	3.46	2.33	1.13	0.082	−0.850	−0.206*
b	0.12	0.12	0.00	0.553	0.12	0.13	0.01	0.347*	0.850	+0.206*
ω_o	0.94	0.89	0.05	0.167	0.94	0.85	0.09	*0.058*	0.815*	−0.418
α_{scat}	2.07	1.91	0.16	***0.041****	2.11	1.87	0.24	***0.001****	+0.984*	−0.612*
α_{abs}	0.33	0.48	0.15	0.099*	0.35	0.79	0.44	***0.001****	+0.495*	***+0.020****

p-values (two-tailed) italicized in bold indicate significance at the 95% confidence interval or greater.
An asterisk (*) indicates values obtained using a parametric test.

among aerosol chemical properties, hygroscopic growth, and precipitation are currently being conducted with a newly acquired Aerosol Mass Spectrometer (Aerodyne, Inc.) and scanning humidograph to investigate this apparent relationship.

Cool season precipitation events were associated with air masses originating primarily in inland areas north-northwest of the study area, with a component originating near the Gulf of Mexico. In the absence of seasonal biogenic emissions, these events exhibited overall lower aerosol optical property values and showed evidence of organic emissions from biomass burning. Cool season frontal precipitation was strongly influenced by air masses originating to the northwest of the study

area, and also from coastal areas near the Gulf of Mexico and the Atlantic Ocean, while cool season non-frontal events were largely characterized by northwest flow snowfall. While consistent with the presence of smaller, biomass burning particles, aerosol properties did not seem to play a role in the intensity of precipitation during the cool season.

Values of α_{abs} consistently and significantly increase from beginning to maturation hour, as well as from light to heavy precipitation, during precipitation events in this study. This trend may have been related to a relatively higher fraction of water soluble organic carbon compounds coalescing and serving as effective CCN during the warm season, which ultimately enhanced precipitation. Another possible explanation for this trend may be the aging and/or mixing state of aerosols impacting AppalAIR during precipitation events in both seasons. Freshly emitted soot particles are more hydrophobic than organic particles (Haywood and Boucher, 2000; Jacobson 2006). However, if organic particles are emitted locally and soot particles are advected from some distance away, the soot particles may experience atmospheric aging and mixing with sulphate particles. This would result in soot particles that are more hygroscopic and scattering than freshly emitted organics. Therefore, the trend in α_{abs} values may have indicated the raining out of coated or mixed soot particles at maturation or during heavy precipitation.

Acknowledgements

The authors gratefully acknowledge the many NWS COOP and CoCoRaHS precipitation observers, as well as the NOAA Air Resources Laboratory (ARL) for the provision of the HY-SPLIT transport and dispersion model (http://www.arl.noaa.gov/ready.php) used in this publication. C. Konrad offered advice in the design of the synoptic classification scheme, and D. Miller, H. Neufeld, and R. Emanuel also offered helpful comments on the research design.

References

Anderson TL, Ogren JA. 1998. Determining aerosol radiative properties using the TSI 3563 Integrating Nephelometer. *Aerosol Science and Technology* **29**: 57–69.

Andreae MO, Rosenfeld D, Artaxo P, Costa AA, Frank GP, Longo KM, Silva-Dias MAF. 2004. Smoking rain clouds over the Amazon. *Science* **303**: 1337–1342.

Barr JG, Fuentes JD, Bottenheim JW. 2003. Radiative forcing of phytogenic aerosols. *Journal of Geophysical Research* **108**(D15): 1–13. DOI: 10.1029/2002JD002978.

Bell TL, Rosenfeld D, Kim KM, Yoo JM, Lee MI, Hahnenberger M. 2008. Midweek increase in U.S. summer rain and storm heights suggests air pollution invigorates rainstorms. *Journal of Geophysical Research* **113**: D02209.

Bergstrom RW, Russell PB, Hignett P. 2002. Wavelength dependence of the absorption of black carbon particles: Predictions and results from the TARFOX experiment and implications for aerosol single scattering albedo. *Journal of the Atmospheric Sciences* **59**: 567–577.

Bollasina M, Nigam S, Lau KM. 2007. Absorbing aerosols and summer monsoon evolution over South Asia: an observational portrayal. *Journal of Climate* **21**: 3221–3239.

Bond TC, Anderson TL, Campbell D. 1999. Calibration and intercomparison of filter-based measurements of visible light absorption by aerosols. *Aerosol Science and Technology* **30**: 582–600.

Borys RD, Lowenthal DH, Cohn SA, Brown WOJ. 2003. Mountaintop and radar measurements of anthropogenic aerosol effects on snow growth and snowfall rate. *Geophysical Research Letters* **30**: 1538.

Brankov E, Rao ST, Porter PS. 1998. A trajectory-clustering-correlation methodology for examining the long-range transport of air pollutants. *Atmospheric Environment* **32**: 1525–1534.

Cifelli R, Doesken N, Kennedy P, Carey LD, Rutledge SA, Gimmestad C, Depue T. 2005. The community collaborative rain, hail, and snow network. *Bulletin of the American Meteorological Society* **86**: 1069–1077.

Delene DJ, Ogren JA. 2002. Variability of aerosol optical properties at four North American surface monitoring sites. *Journal of the Atmospheric Sciences* **59**: 1135–1150.

Dorling SR, Davies TD, Pierce CE. 1992. Cluster analysis: a technique for estimating the synoptic meteorological controls on air and precipitation chemistry-Results from Eskdalemuir, South Scotland. *Atmospheric Environment* **26A**: 2583–2602.

Draxler RR. 1999. HYSPLIT4 user's guide, NOAA Tech. Memo, ERL ARL-230, NOAA Air Resources Laboratory, Silver Spring, MD.

Draxler RR, Rolph GD. 2011. HYSPLIT (HYbrid single-particle Lagrangian integrated trajectory) model access via NOAA ARL READY. Available at http://ready.arl.noaa.gov/HYSPLIT.php, NOAA Air Resources Laboratory, Silver Spring, MD.

Givati A, Rosenfeld D. 2004. Quantifying precipitation suppression due to air pollution. *Journal of Applied Meteorology* **43**: 1038–1056.

Givati A, Rosenfeld D. 2005. Separation between cloud-seeding and air-pollution effects. *Journal of Applied Meteorology* **44**: 1298–1314.

Goldstein AH, Koven CD, Heald CL, Fung IY. 2009. Biogenic carbon and anthropogenic pollutants combine to form a cooling haze over the southeastern United States. *Proceedings of the National Academy of Sciences* **106**: 8835–8840.

Haywood J, Boucher O. 2000. Estimates of the direct and indirect radiative forcing due to tropospheric aerosols: A review. *Reviews of Geophysics* **38**: 513–543.

Holben BN, Tanré D, Smirnov A, Eck TF, Slutsker I, Abuhassan N, Newcomb WW, Schafer JS, Chatenet B, Lavenu F, Kaufman YJ, Vande Castle J, Setzer A, Markham B, Clark D, Frouin R, Halthore R, Karneli A, O'Neill NT, Pietras C, Pinker RT, Voss K, Zibordi G. 2001. An emerging ground-based aerosol climatology: aerosol optical depth from AERONET. *Journal of Geophysical Research* **106**(D11): 12.067–12.097.

Jacobson MZ. 2006. Effects of externally-through-internally-mixed soot inclusions within clouds and precipitation on global climate. *Journal of Physical Chemistry A* **110**: 6860–6873.

Jirak IL, Cotton WR. 2005. Effect of air pollution on precipitation along the Front Range of the Rocky Mountains. *Journal of Applied Meteorology and Climatology* **45**: 236–245.

Karl TR, Melillo JM, Peterson TC. 2009. *Global Climate Change Impacts in the United States*. Cambridge University Press: New York.

Keighton S, Lee L, Holloway B, Hotz D, Zubrick S, Hovis J, Votaw G, Perry LB, Lackmann G, Yuter S, Konrad CE, Miller D, Etherton B. 2009. A collaborative approach to better understanding northwest flow snowfall in the southern Appalachians. *Bulletin of the American Meteorological Society* **90**: 979–991.

Keim BD. 1996. Spatial, synoptic, and seasonal patterns of heavy rainfall in the southeastern United States. *Physical Geography* **17**: 313–328.

Kelly GM, Perry LB, Taubman BF, Soulé PT. 2012. Synoptic Classification of Precipitation Events in the Southern Appalachian Mountains. *Climate Research* **55**: 1–15.

Khain A, Pokrovsky A, Pinsky M. 2004. Simulation of effects of atmospheric aerosols on deep turbulent convective clouds using a spectral microphysics mixed-phase cumulus cloud model. Part I: model description and possible applications. *Journal of the Atmospheric Sciences* **61**: 2963–2982.

Konrad CE. 1997. Synoptic-scale features associated with warm season heavy rainfall over the interior southeastern United States. *Weather and Forecasting* **12**: 557–571.

Li W, Li L, Fu R, Deng Y, Wang H. 2010. Changes to the north Atlantic subtropical high and its role in the intensification of summer rainfall variability in the southeastern United States. *Journal of Climate* **24**: 1499–1506.

Lohmann U, Hoose C. 2009. Sensitivity studies of different aerosol indirect effects in mixed-phase clouds. *Atmospheric Chemistry and Physics* **9**: 15049–15081.

Lynn BH, Healy R, Druyan LM. 2007. An analysis of the potential for extreme temperature change based on observations and model simulations. *International Journal of Climatology* **20**: 1539–1554.

National Centers for Environmental Prediction Daily Weather Maps. 2012. Available at http://www.hpc.ncep.noaa.gov/dailywxmap/index.html, Accessed January 12, 2011.

National Climatic Data Center Service Records Retention System Analysis and Forecast Charts. 2010. Available at http://nomads.ncdc.noaa.gov/ncep/NCEP, Accessed January 12, 2011.

Perry LB, Konrad CD, Schmidlin TW. 2007. Antecedent upstream air trajectories associated with northwest flow snowfall in the southern Appalachians. *Weather and Forecasting* **22**: 334–35.

Perry LB, Konrad CE, Hotz DG, Lee LG. 2010. Synoptic classification of snowfall events in the Great Smoky Mountains, USA. *Physical Geography* **31**: 156–171.

Power HC, Sheridan SC, Senkbeil JC. 2006. Synoptic climatological influences on the spatial and temporal variability of aerosols over North America. *International Journal of Climatology* **26**: 732–741.

Prados AI, Dickerson RR, Doddridge BG, Milne PA, Moody JL, Merrill JT. 1999. Transport of ozone and pollutants from North America to the North Atlantic Ocean during the 1996 Atmosphere/Ocean Chemistry Experiment (AEROCE) intensive. *Journal of Geophysical Research* **104**: 26219–26233. DOI: 10.1029/1999JD900444.

Rosenfeld D. 1999. TRMM observed first direct evidence of smoke from forest fires inhibiting rainfall. *Geophysical Research Letters* **26**: 3105–3108.

Rosenfeld D. 2000. Suppression of rain and snow by urban and industrial air pollution. *Science* **287**: 1793.

Rosenfeld D, Givati A. 2006. Evidence of orographic precipitation suppression by air pollution induced aerosols in the western United States. *Journal of Applied Meteorology and Climatology* **45**: 893–911.

Rosenfeld D, Lahav R, Khain A, Pinsky M. 2002. The role of sea spray in cleansing air pollution over ocean via cloud processes. *Science* **297**: 1667–1670.

Rosenfeld D, Dai J, Yu X, Yao Z, Xu X, Yang X, Du C. 2007. Inverse relations between amounts of air pollution and orographic precipitation. *Science* **315**: 1396–1398.

Rudich Y, Khersonsky O. 2002. Treating clouds with a grain of salt. *Geophysical Research Letters* **29**: 2060.

Sheridan PJ, Delene DJ, Ogren JA. 2001. Four years of continuous surface aerosol measurements from the DOE/ARM Southern Great Plains CART site. In Eleventh ARM Science Team Meeting Proceedings. Atlanta, GA, March 19–23.

Swap RM, Garstang M, Greco S, Talbot R, Kållberg P. 1992. Saharan dust in the Amazon Basin. *Tellus* **44B**: 133–149.

Taubman BF, Hains JC, Thompson AM, Marufu LT, Doddridge BG, Stehr JW, Piety CA, Dickerson RR. 2006. Aircraft vertical profiles of trace gas and aerosol pollution over the mid-Atlantic Unites States: Statistics and meteorological cluster analysis. *Journal of Geophysical Research* **111**: D10S07.

U.S. Census Bureau. 2010. 2006–2010 American Community Survey. Available at http://www.census.gov/acs/www/, Accessed January 3, 2012.

Weber RJ, Sullivan AP, Peltier RE, Russell A, Yan B, Zheng M, Gouw J, Warneke C, Brock C, Holloway JS, Atlas EL, Edgerson E. 2007. A study of secondary organic aerosol formation in the anthropogenic-influenced southeastern United States. *Journal of Geophysical Research* **112**: D13302.

Zubler EM, Lohmann U, Lüthi D, Schär C, Muhlbauer A. 2011. Statistical analysis of aerosol effects on simulated mixed-phase clouds and precipitation in the Alps. *Journal of the Atmospheric Sciences* **68**: 1474–1492. DOI: 10.1175/2011JAS3632.1.